Gated pinhole camera imaging of the high-energy ions emitted by a discharge produced Sn plasma for extreme ultraviolet generation

Gated pinhole camera imaging of the high-energy ions emitted by a discharge produced Sn plasma for extreme ultraviolet generation

K. Gielissen,[1,a)] Y. Sidelnikov,[2] D. Glushkov,[3] W. A. Soer,[4] V. Banine,[3] and J. J. A. M. v. d. Mullen[1]
[1]*Eindhoven University of Technology, Den Dolech 2, 5600 MB Eindhoven, The Netherlands*
[2]*ISAN Institute of Spectroscopy, Fizicheskaya Str. 5, Troitsk, Moscow Region 142190, Russia*
[3]*ASML, De Run 6501, 5504 DR Veldhoven, The Netherlands*
[4]*Philips Research, High Tech Campus 4, 5656 AE Eindhoven, The Netherlands*

(Received 23 June 2009; accepted 3 September 2009; published online 20 October 2009)

The origin and nature of the high-energy ions emitted by a discharge produced plasma source are studied using gated pinhole camera imaging. Time-of-flight analysis in combination with Faraday cup measurements enables characterization of the high-velocity component of the ionic debris. The use of an optional magnetic field allows mass-to-charge analysis of the first part of the Faraday cup signal. It is shown that this consists mainly of oxygen ions emitted from a region near the cathode. Time-resolved images of Sn ions with a kinetic energy of 45 keV visualize the regions in between the electrodes where the high-energy ion generation takes place. © *2009 American Institute of Physics*. [doi:10.1063/1.3239994]

I. INTRODUCTION

To fulfill the demand for smaller and faster electronic devices, the feature size in semiconductor industry has to be reduced. To that end, future lithography tools have to make use of extreme ultraviolet (EUV) radiation to project small-scale patterns onto wafers. This new technology will employ plasma sources to produce the desired radiation at 13.5 nm. With the use of a collector mirror the light from these plasma sources is collected and focused onto the entry point of the lithographic system, the intermediate focus. Apart from the EUV radiation, these sources also produce debris that can damage the collector optics and result in reflection losses.

One of the two types of EUV plasma sources, a Sn-based discharge produced plasma (DPP) source, is used as a light source for the installed Alpha Demo Tool scanners from ASML.[1–5] One of the main challenges in maintaining productivity has proven to be the lifetime of the collector optics in the source-collector assembly. Besides Sn deposition, the major factor determining the lifetime of the collector is ion sputtering of the collector surface. These ions are produced by the plasma.

Previously, the characteristics of ions emitted by a Sn-based DPP source were investigated using time-of-flight (TOF) velocity measurements in combination with an electrostatic spectrometer and Faraday cup (FC).[6–8] It was shown that suprathermal Sn ions with kinetic energies up to 100 keV are emitted by the plasma. The presence of ions with a higher velocity is also detected, but the nature of these ions was not identified. Therefore, it is essential to investigate the origin and nature of the high-velocity ions emitted by the EUV producing DPP.

This paper will report on gated pinhole camera imaging of the high-energy ion beam emitted by a DPP source. First, the plasma source used for the experiments will be described followed by an explanation of the time-resolved imaging technique. Next, we discuss the images by comparison to the simultaneously recorded FC signal. The mass-to-charge ratio of the ions from the first part of the ion beam is calculated by measuring the deflection by a magnetic field. Finally, time-resolved images of highly energetic Sn ions show the positions in between the electrodes where the ions are produced. These highly energetic Sn ions have energies in the range of 45 keV.

II. EXPERIMENTAL SETUP

A Sn-based DPP source, developed at the Russian Institute of Spectroscopy (ISAN), is used to investigate the origin of the high-energy ion beam. Figure 1 shows a schematic top view of the source. The source consists of two disk electrodes, rotating through a bath of liquid Sn in a vacuum environment. A high voltage of about 4 kV is applied across the discharge gap (~3–4 mm) with the use of a capacitor bank. Hence, an electric energy of ~4 J is applied to the

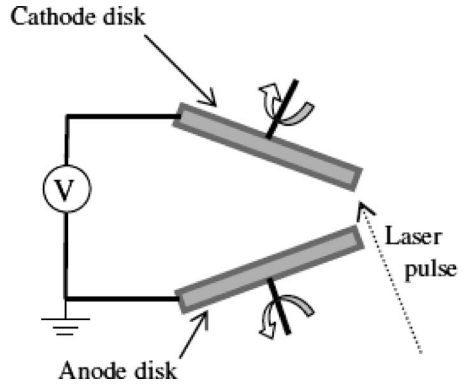

FIG. 1. Schematic of the top view of the DPP source. Two rotating disk electrodes are covered with liquid Sn. First, a negative voltage is applied to the cathode followed by a laser pulse evaporating the liquid Sn in between the electrodes and initiating the discharge.

[a)]Electronic mail: k.gielissen@tue.nl.

plasma. To ignite the discharge a *Q*-switched pulsed Nd:YAG (yttrium aluminum garnet) laser, operating at a wavelength of 1064 nm with a pulse energy of 15 mJ and a pulse width of 15 ns, is focused onto the cathode surface. As a consequence a partly ionized Sn vapor expands to the anode, and when the density is sufficiently high, the discharge is initiated. The current through the plasma increases rapidly (~100 ns) up to a maximum of roughly 20 kA, and due to the Lorentz forces the plasma compresses in a radial direction and a multiply ionized Sn plasma is formed. Due to the radiative collapse[9] of high *Z* plasmas, a micropinch develops that emits the desired EUV radiation. Finally, the plasma expands into vacuum and decays. The observed lifetime of a micropinch in DPP sources equals about 10 ns.

Some typical plasma characteristics of an EUV emitting Sn-based discharge plasma can be found in Refs. 10 and 11. Although the source depicted in Fig. 1 has a different electrode configuration, the main plasma characteristics are similar. During the pinch phase the electron temperature and the electron density may rise locally up to, respectively, $T_e = 35$ eV and $n_e = 3 \times 10^{25}$ m^{-3}. When performing TOF analysis of the ion beam, the micropinch can be used as the zero point on the time scale, as the high density plasma is only short lived and it can easily be identified by the high radiation emission or the sudden decrease in the discharge current.

In order to visualize the origin of the ion beam, a multichannel plate (MCP) detector with an image intensifier and a phosphorus screen has been used. A similar experimental setup has previously been used to resolve the different phases of a DPP during the discharge cycle.[12] At that time, the MCP was initially intended to detect EUV photons as the plasma evolution with high time resolution in the EUV range was investigated. However, the MCP detector is also sensitive to high-energy ions.[13] Moreover, it has been shown that when the ion impact energy is sufficiently high (>3 keV), heavy ions are detected with equal efficiency as low mass ions.[14–16] This justifies that with the use of the gated MCP, time-resolved images can be made of the ion beam.

To perform TOF analysis, the gating pulse has to be send to the MCP at the expected arrival time *t* of the ions. Therefore a delay generator is connected to the gating pulse generator to introduce a time delay *t* between the pinch and the gating pulse. From the travel distance *D* and arrival time *t*, the velocity of the ions can be computed and from their mass the kinetic energy *E* can be calculated. A graph showing the delay pulse in combination with the derivative of the discharge current and the trigger laser pulse is depicted in Fig. 2. First the laser pulse ignites the discharge. The discharge starts and at maximum current the plasma pinches. This moment is chosen to be zero on the time scale. The gating pulse for a time delay of $t = 1$ μs is shown.

At the time that the MCP is open, typically 1 μs after the discharge pulse, some light may still be emitted by the extinguishing plasma. To distinguish between photons and ions or even electrons detected by the MCP, a magnetic field can be applied perpendicular to the direction of the ion beam. This allows to investigate the nature of the detected particles and to perform mass-to-charge analysis. The pinhole camera

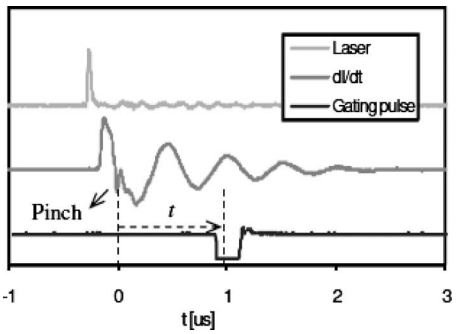

FIG. 2. The gating pulse for time delay $t = 1$ μs is shown together with the laser pulse and the time derivative of the discharge current dI/dt. The pinch is taken as zero on the time scale.

consists of a pinhole with a diameter of 250 μm, a MCP image intensifier made at ISAN, and a commercial digital camera. The pinhole image is projected onto the surface of the MCP, intensified, and converted into visible light by a phosphorus screen. Here the image is recorded by a digital camera. The MCP is placed at a distance $D = 88$ cm from the discharge plasma. Figure 3 shows a schematic of the setup. The MCP is gated with a fast 4 kV high voltage pulse over the plate and the adjacent gap to the phosphorus screen. The typical duration of the gating pulse is 200 ns. An optional magnetic field of 35 mT can be applied behind the pinhole, perpendicular to the direction of the ion beam.

A FC is mounted to the source chamber at the same distance from the plasma as the MCP detector. In order to suppress secondary electron formation in the region close to cup, an extra limiting aperture of 8 mm was placed in between the discharge plasma and the cup. A typical FC signal shows the ion beam current as a function of time. More details about the FC configuration can be found in Ref. 6. The FC signal is recorded simultaneously with the Charge Coupled Device (CCD) image. Again, the time of the pinch is chosen to be zero on the time scale. From the travel distance *D* and arrival time *t*, the velocity of the ions can be computed and from their mass the kinetic energy E_{kin} can be calculated.

Concluding, each CCD image shows the photons and highly energetic particles captured during an adjustable time interval of 200 ns and emitted during one single discharge in

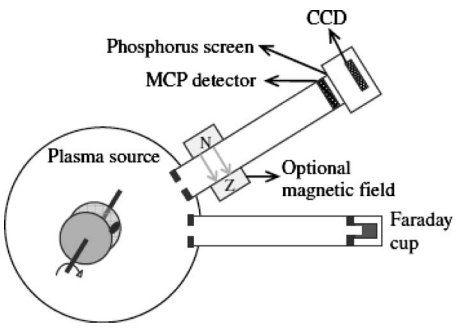

FIG. 3. The time-resolved pinhole image is recorded simultaneously with the FC signal. The distance of the detectors to the discharge plasma is chosen to be equal to 88 cm. For the MCP detector an aperture of 0.25 mm and for the FC an 8 mm aperture are placed. An optional magnetic field can be applied perpendicular to the path of the ion beam.

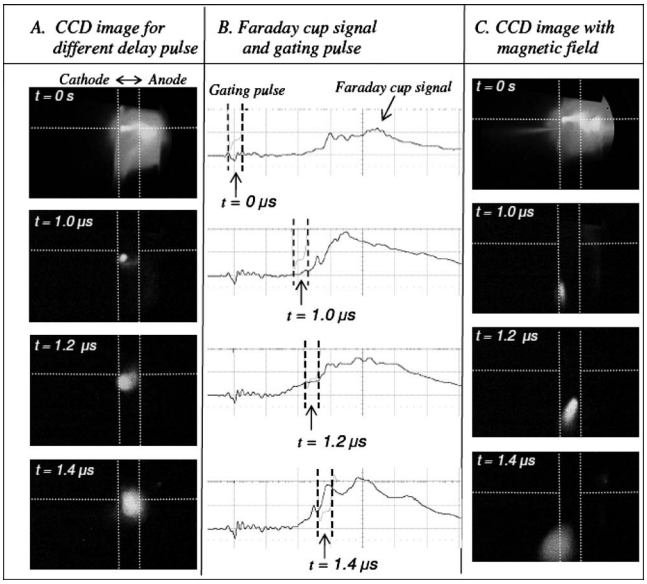

FIG. 4. (a) The CCD images for different time delays t between the discharge and the gating pulse. The position of the electrodes is marked by dotted lines. (b) Oscilloscope pictures of the FC signal measured simultaneously with the gating MCP pulse from the images of (a). (c) CCD images with a magnetic field of 35 mT applied perpendicular to the particles' trajectory. From the downwards shift of the spot it can be concluded that ions are being captured with the MCP.

radial direction. From the time delay, which is equal to the TOF of the particles, the velocity and thus their kinetic energy can be calculated. Simultaneously with the CCD image, a FC cup signal is recorded from ions also emitted to the front side. By projecting the delay pulse of the MCP on the simultaneously recorded FC signal trace, one can see which part of the ion beam is visualized by the pinhole camera. Thus, by changing the delay time, a velocity range of the ion beam can be chosen and the region of production is visualized.

III. ION BEAM ANALYSIS

First, the position of the electrode gap has to be identified in the CCD images. Therefore, a pinhole image is made with no time delay between the discharge and the gating pulse. Due to the width of the gating pulse and since no spectral filter is used in front of the pinhole, this picture shows a time-integrated image of the emitted radiation during the discharge. This allows identifying the position of the electrodes. These are marked by the dotted lines in Fig. 4. Next, pictures are made for delay pulses of 1.0, 1.2, and 1.4 μs. In these pictures photons are not expected. Figure 4(a) shows the resulting pictures. Simultaneously with the CCD images, the FC signal was recorded with an oscilloscope as shown in Fig. 4(b). The time delay t between the pinch and the gating pulse is indicated on the trace of the FC signal by the arrow, and the gating pulse interval is displayed by the dashed lines.

Figure 4(b) clearly shows that there is a substantial difference between the individual FC signals. This shows that while the discharge conditions are similar, the ion energy distribution in the direction of the measurement tools differs from pulse to pulse. Finally, a magnetic field was applied perpendicular to the ion beam direction, and a series of CCD images with the same time-delay settings as mentioned above was made. These pictures are shown in Fig. 4(c). Hereafter we will discuss the images in Fig. 4 for the different delay times in more detail.

(1) $t=0$ μs. The first picture in Fig. 4(a) shows almost no difference with the first one in Fig. 4(c), where the magnetic field is applied. Apart from the wide low intensity signal, of which the shape differs from pulse to pulse, no substantial difference can be seen for the bright spots in between the electrodes. Thus, it can be concluded that this bright spot is an image of the radiation emitted by the discharge plasma during the first 200 ns of the discharge. The narrow area with high intensity close to the cathode surface clearly shows the position of the pinch. This area of high intensity widens toward the anode surface and it even surrounds the anode surface. To understand these phenomena we follow the discharge plasma evolution as described in Ref. 10. There can be two possible origins of the radiation emitting plasma close to the anode surface. First, due to the Lorentz forces, the plasma is confined in the radial, but not in the axial direction. Because the pinch is positioned close to the cathode surface, the plasma can escape more easily in the anode direction. Second, at a time of 50–80 ns after the pinch, a *second* light-emitting plasma was observed expanding from the cathode to anode.[10] In both cases there is a possibility that the light-emitting plasma surrounds the anode surface. This explains the MCP signal from this region of the plasma source. The FC signal from Fig. 4(b) shows a small negative signal at the time of the pinch. This may be due to the collection of secondary electrons, which are produced by the plasma radiation in a region close to the cup. The large positive signal represents the ion beam, which is collected by the cup. The dashed lines show the gating pulse width during which the CCD image was made. As stated above, the FC signals from Fig. 4(b) are measured simultaneously with the images from Fig. 4(a).

(2) $t=1.0$ μs. A bright spot can be seen close to the cathode surface in Fig. 4(a). When the magnetic field is applied perpendicular to the particles' trajectory just behind the aperture as shown in Fig. 3, the signal in between the electrodes has fully disappeared as can be seen from the second picture in Fig. 4(c). Instead, an elongated spot appears at the bottom of the picture. As photons are not deflected by a magnetic field, this shows that at 1 μs after the pinch no detectable radiation is emitted by the DPP source. Furthermore, the downwards shift of the spot shows that the signal is due to the imaging of ions, as electrons would have been deflected upwards. It can be concluded that a beam of high-energy ions, which contribute to the first part of the FC signal as seen in Fig. 4(b), is emitted from the cathode region. Moreover, the deflection distance is a measure of the mass-to-charge ratio m/q of the ions. The elongation of the spot shows that the ions with TOF=1 μs have different m/q val-

ues. Ions with low m/q will be deflected more when traveling through a magnetic field than ions with higher m/q values. The mass-to-charge analysis of the deflected ions will be treated in Sec. IV. Figure 4(b) shows that the positive FC signal trace, which represents the ion beam, starts at about 1 μs after the discharge. The position of the gating pulse coincides with the arrival of the first part of the ion beam. Thus, ions with a velocity $v=8.8\times10^5$ m/s are imaged and they originate from the same region as where the pinch was observed, namely close to the cathode surface.

(3) $t=1.2$ μs. By comparison of the third picture in Fig. 4(a) with the third one in Fig. 4(c) in a similar reasoning as above, it can be concluded that no photons but a beam of ions with a velocity of $v=7.3\times10^5$ m/s is imaged by the MCP detector. The width of the beam is increased in size. It can also be seen that the downwards shift of the bright spot is slightly less than in the picture above. Although these ions have a lower velocity, which would result in a higher deflection because of the magnetic field, some of them must have a significant higher m/q value. Thus, assuming that the ions have an equal mass, it is expected that these ions will have a lower charge. From Fig. 4(b) it can be seen that the FC signal integrated over the gating pulse is higher than at $t=1$ μs delay time. Because of the lower charge, the number of ions captured during this time interval has to be increased. This may explain the observed beam widening as the higher ion number density may result in an increased Coulomb interaction between the ions.

(4) $t=1.4$ μs. From the last picture in Figs. 4(a) and 4(c) and the TOF it can again be concluded that a beam of ions with a velocity $v=6.3\times10^5$ m/s is imaged. It proves to be difficult, however, to distinguish the origin of the ion beam as the spot has widened and covers the whole electrode gap. Figure 4(b) shows that the integrated FC signal over the gating pulse has increased even further, meaning that the number density of the ions has again increased. Therefore, the widening of the spot is probably due the Coulomb interaction of the high number of ions passing through the aperture. Although the velocity of the ions is lower, the minimum downwards shift of the spot has not changed with respect to the previous picture. This shows that the imaged ions on average must have a higher m/q value than the ions from the previous picture. Again, assuming that the mass is equal, these ions are expected to have a lower charge.

Concluding, the deflection of the spot with a magnetic field shows that the spot seen on the CCD images for $t>0$ s is the result of the capturing of ions. From comparison with the FC signal the origin of the first part of the high-energy ion beam is identified as being close to the cathode surface. These ions have velocity $v>7\times10^5$ m/s. In Sec. IV, a calculation will be made of the mass-to-charge ratio based on the lateral deflection of the spot from Fig. 4(c).

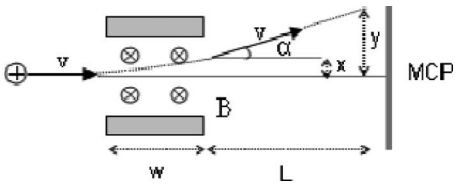

FIG. 5. A schematic presentation of the model used to calculate the deflection y at the MCP position at a distance L behind a perpendicular applied magnetic field B. A positive ion with speed v entering the magnetic field B of length w will exit the field under angle α.

From this it is possible to analyze the ion species that are visualized with the MCP detector.

IV. MASS-TO-CHARGE RATIO

With the use of a simple analytical model that describes the path of a charged particle passing a magnetic field of finite length w, the mass-to-charge ratio of the deflected ions from Fig. 4(c) can be calculated. The parameters used in this model are shown schematically in Fig. 5.

The magnetic field B is assumed to be uniform over a finite length w, and zero elsewhere. An ion with speed v moving through a perpendicular magnetic field B will travel a circular path with radius R, given by

$$R=\frac{m\times v}{q\times B}, \tag{1}$$

where m is the mass and $q=Z\times e$ is the charge of the ion with charge number Z. The speed of this ion can be calculated from the TOF t and the distance D between the detector and the source using $v=D/t$. As long as the condition $w<R$ holds the ion will leave the magnetic field at an angle α and it will collide with the MCP detector placed a distance L behind the magnetic field. The lateral deflection y of the ion is then equal to $y=x+L\times\tan(\alpha)$. From trigonometry it follows that $\sin(\alpha)=w/R$ and $x=R\times[1-\cos(\alpha)]$. The mass-to-charge ratio m/q of this ion can now be derived using Eq. (1) as

$$\frac{m}{q}=\sqrt{y^2+L^2}\times\left(\frac{B\times w\times t}{y\times D}\right). \tag{2}$$

To facilitate the identification of the ion species the m/q ratio is expressed in atomic-mass-unit M versus ionic charge number Z. From the CCD images in Fig. 4(c) the lateral deflection y with respect to the center of the original spot is measured. For each time delay t the minimum, the maximum, and the average deflection distance y are measured. With the use of Eq. (2) the mass-to-charge ratio M/Z of the deflected ions is calculated and plotted in Fig. 6 together with the resultant measurement error.

(1) $t=1.0$ μs. These ions have a deflection distance of about 1.4 cm$<y<$2.4 cm. Figure 6 shows that with Eq. (2) a mass-to-charge ratio of $3<M/Z<7$ is calculated. It is expected that these ions will be oxygen (^{16}O) with charges $Z=3$ and $Z=4$, as unrealistically high charge states would be needed for Sn ions to have such a low M/Z ratio.[17] These oxygen ions have a kinetic

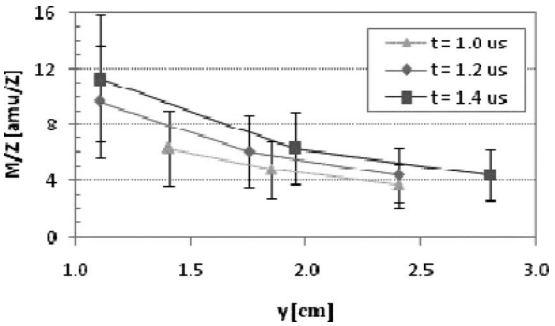

FIG. 6. The mass-to-charge ratio M/Z calculated with Eq. (2) as a function of the lateral deflection distance y from the bright spots in Fig. 4(c).

energy $E_{kin}=65$ keV, and the origin is located close to the cathode surface, as shown in Fig. 4(a).

(2) $t=1.2$ μs. As pointed out in Sec. III, these ions not only have a lower velocity but also a smaller minimum deflection distance 1.1 cm$<y<$2.4 cm, which results in a higher maximum M/Z value. Figure 6 shows the result with $4<M/Z<10$. The ions having a value of $M/Z>7$ may consist of Sn ions (^{118}Sn) with charges $Z=12$ up to $Z=15$. However, the imaged ions have a velocity of $v=7.3\times10^5$ m/s, which would result in a kinetic energy of 331 keV for Sn ions. This is an extremely high value in view of the fact that previously the detection of energies only up to 100 keV is assumed.[6] Thus, it is expected that the imaged ions are all oxygen (^{16}O), they then have charges $Z=2$ up to $Z=4$, taken the error into account. The imaged oxygen ions have a kinetic energy of about 45 keV and their origin is located near the cathode surface.

(3) $t=1.4$ μs. Again, these ions have a lower velocity but the minimum deflection distance has not changed with respect to the previous image, 1.1 cm$<y<$2.8 cm resulting in a mass-to-charge ratio of $4<M/Z<12$. As seen in Fig. 6 a larger part of the ions have a value of $M/Z>7$. These ions may consist of ^{118}Sn with charges $Z=10$ up to $Z=15$ and a kinetic energy of 243 keV.

However, in the same reasoning as above, it is expected that these ions will be ^{16}O with charges $Z=1$ up to $Z=4$ and with $E_{kin}=33$ keV. The origin of these ions cannot be determined from the image in Fig. 4(a) due to the increase in the spot diameter.

It should be noted that the previously followed reasoning does not exclude that the ions with $M/Z>7$ may be highly charged Sn ions with extremely high kinetic energies. In order to identify the ion species more accurately, a spectrometer with deflection voltages in the range of tens of kilovolts is required.

The oxygen measured in this experiment is most likely introduced into the plasma because of laser evaporation of oxidized Sn at the cathode surface. The oxidation of Sn inside the source chamber takes place while opening the vacuum chamber in between experiments and is hard to avoid. It is expected that after a large number of discharges the oxidized Sn will be consumed so that oxygen will no longer be present among the ion beam.

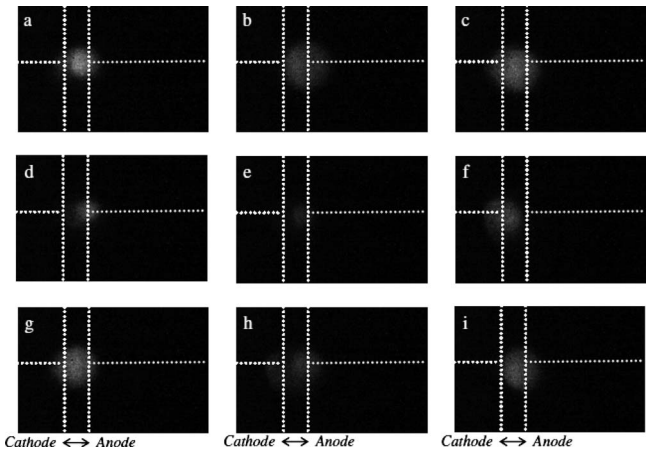

FIG. 7. Time-resolved pinhole images of the high-energy ion beam emitted by single discharge pulses. The spots are the result of the collection of Sn ions with TOF equal to 3 μs during a time interval of 200 ns. These ions have kinetic energies of 45 keV and may originate from the cathode region (f), the middle of the discharge gap [(c), (g), and (i)], as well as the anode region [(a), (b), (d), and (e)].

V. ORIGIN OF THE HIGH-ENERGY SN IONS

To identify the origin of the beam of high-energy Sn ions, MCP pictures have to be made of a beam that is free of contamination. However, a high number of discharge pulses will produce a significant amount of debris that can obstruct the pinhole, and, thus, it is not advisable to wait until the oxidized Sn is consumed completely. Therefore we have made time-integrated pinhole images of that part of the ion beam where the presence of high-energy Sn ions is experimentally confirmed.

Measurements of the high-energy ion beam with an ion spectrometer have shown that Sn ions with $E/Z=4.9$ keV are detected.[6] These Sn ions have charge numbers from $Z=1$ up to $Z=15$, resulting in a maximum measured energy of $E_{kin}=75$ keV. As the average charge number of these high-energy ions equals to 8, which equals to about 40 keV, a large amount of Sn ions with kinetic energy of 45 keV in the high-energy ion beam is to be expected. With the MCP detector positioned at 80 cm, these ions will have a TOF in the order of 3 μs.

However, as mentioned previously, the images of ions with a TOF larger than 1.4 μs show a large wide spot, and no information about the origin can be obtained. The widening of the spot increases even more for a larger TOF. Because of the higher number of ions as seen from the FC signal, the Coulomb interaction between the ions increases and widens the spot. To reduce the number of ions, the size of the aperture was reduced to 100 μm. It was also positioned further away from the discharge plasma to reduce the image magnification.

Figure 7 shows nine CCD images of the Sn ions with $E_{kin}=45$ keV. Each image shows the ions, emitted during one single discharge, that are detected by the MCP during a time interval of 200 ns at 3 μs after the pinch. The dotted lines show the position of the electrodes, which is determined by a reference picture without a delay pulse, in the same manner as stated above. Although the images were recorded under identical discharge conditions, each image

shows a spot with different intensity and different diameter. Similar to the FC signals from Fig. 4(b), the ion emission shows a significant difference from pulse to pulse. Furthermore, the position of the spot is not restricted to a single place in between the discharge gap. Figure 7(f) clearly shows a spot close to the cathode surface, while Figs. 7(a), 7(b), 7(d), and 7(e) show a spot close to the anode surface. The other pictures, Figs. 7(c), 7(g), and 7(i), show a spot in front of the center of the electrode gap.

It can be concluded that during each discharge the intensity of the emitted high-energy beam is different. Furthermore, because the beam originates from different places in the discharge gap, different mechanisms may be responsible for the high-energy ion emission.

VI. CONCLUSION AND OUTLOOK

By means of TOF analysis the gated pinhole images are compared with simultaneously recorded FC signals. It is shown that the ions emitted by the DPP source with velocity $v > 7 \times 10^5$ m/s originate from a region close to the cathode surface. These ions contribute to the first part of the FC signal. An optional magnetic field perpendicular to the path of the ions is employed to perform mass-to-charge analysis. The ions are identified as oxygen with energies from $E_{\mathrm{kin}} = 45$ keV up to $E_{\mathrm{kin}} = 65$ keV, and charge number from $Z = 2$ to $Z = 4$.

For ions with velocity $v \sim 6.3 \times 10^5$ m/s the origin is unclear. These ions are expected to be oxygen with $E_{\mathrm{kin}} = 33$ keV and $Z = 1$ to $Z = 4$. However, from the mass-to-charge analysis, it cannot be excluded that high-energy Sn ions with $E_{\mathrm{kin}} = 243$ keV and $Z = 10$ to $Z = 15$ are detected. In order to identify Sn ions with these extreme energies, a spectrometer with deflection voltages in the range of several tens of kilovolts is required.

The oxygen ions emitted by the DPP source are expected to be introduced inside the Sn plasma due to evaporation of oxidized Sn from the cathode surface with the Nd:YAG laser pulse. The oxidized Sn will be consumed after a number of discharges and hence is only temporally present among the debris. For the experiments presented here, a large number of discharges may result in the obstruction of the pinhole.

Therefore, it is chosen to make time-integrated pinhole images of Sn ions with velocity $v = 2.7 \times 10^5$ m/s, which corresponds to an energy $E_{\mathrm{kin}} = 45$ keV. The presence of these Sn ions among the debris was experimentally shown with an ion spectrometer.[8] The MCP images showed that these ions originate from a region close to the cathode surface, from the middle of the discharge gap, as well as from a region close to the anode surface.

Some production mechanisms of suprathermal particles by Z-pinch plasmas are discussed in literature.[18] These mechanisms include (1) *compressional heating* of the plasma material inside the micropinch, (2) acceleration due to the formation of *high-inductive electric fields* during the pinch induced current breakup, and (3) *stochastic acceleration* of the tails of the ion distribution function. It is also mentioned that these mechanisms may act simultaneously.

Based on the results presented in this paper, it is expected that several of these mechanisms are responsible for the suprathermal Sn ion production. It is conceivable that the suprathermal ions emitted from the region near the cathode are produced by compressional heating of plasma material inside the pinch. In addition, because of the shrinking plasma column during the micropinch formation[9] an active resistance is introduced inside the discharge circuit on a time scale of ~10 ns. This results in a sudden decrease in the discharge current, and a high-inductive electric field develops to sustain the current. In the anode region, the conditions for the ion-acoustic instability may be satisfied.[18] Hence, anomalous resistivity develops in the plasma near the anode resulting in microinstabilities and possibly high-inductive fields.

A more detailed discussion about these production mechanisms requires an analysis of the Z-pinch dynamics. This is beyond the scope of this paper, but is strongly advised for future investigations focused on suppression of high-energy ion emission.

[1] H. Meiling, S. Lok, B. Hultermans, E. van Setten, B. Pierson, K. Cummings, C. Wagner, and N. Harned, International Extreme UltraViolet Lithography (EUVL) Symposium, Lake Tahoe, CA, 28 September–1 October 2008 (unpublished).
[2] M. Corthout, M. Yoshioka, International EUVL Symposium, Lake Tahoe, CA, 28 September–1 October 2008 (unpublished).
[3] E. Wagenaars, A. Mader, K. Bermann, J. Jonkers, and W. Neff, IEEE Trans. Plasma Sci. **36**, 1280 (2008).
[4] V. Banine, O. Frijns, and G. Swinkels, International Extreme UltraViolet Lithography (EUVL) Symposium, Sapporo, Japan, October 2007 (unpublished).
[5] J. Benschop, V. Banine, S. Lok, and E. Loopstra, J. Vac. Sci. Technol. B **26**, 2204–2207 (2008).
[6] V. Medvedev, R. Gayzoe, V. Krivtsun, V. Ivanov, and K. Koshelev, *Comparison of Spectra of Accelerated Ions Produced by LPP and DPP*, 23rd Symposium on Plasma Physics and Technology, Prague, Czech Republic, 16–19 June 2008 (unpublished).
[7] G. Zukakishvili, V. Krivtsun, V. Gomozov, V. Ivanov, I. Kharkin, D. Glushkov, and K. Koshelev, *Generation of Fast Ions in Vacuum Sparks*, 23rd Symposium on Plasma Physics and Technology, Prague, Czech Republic, 16–19 June 2008 (unpublished).
[8] K. Gielissen, Y. Sidelnikov, D. Glushkov, W. A. Soer, V. Banine, and J. J. A. M. v. d. Mullen, "Characterization of ion emission of an extreme ultraviolet generating discharge produced Sn plasma," J. Appl. Phys. (submitted).
[9] K. N. Koshelev and N. R. Pereira, J. Appl. Phys. **69**, R21 (1991).
[10] E. R. Kieft, J. J. A. M. van der Mullen, G. M. W. Kroesen, V. Banine, and K. N. Koshelev, Phys. Rev. E **71**, 026409 (2005).
[11] E. R. Kieft, J. J. A. M. van der Mullen, and V. Banine, Phys. Rev. E **72**, 026415 (2005).
[12] E. R. Kieft, J. J. A. M. van der Mullen, G. M. W. Kroesen, and V. Banine, Phys. Rev. E **68**, 056403 (2003).
[13] J. L. Wiza, Nucl. Instrum. Methods **162**, 587 (1979).
[14] B. Brehm, J. Grosser, T. Ruscheinski, and M. Zimmer, Meas. Sci. Technol. **6**, 953 (1995).
[15] H. C. Straub, M. A. Mangan, B. G. Lindsay, K. A. Smith, and R. F. Stebbings, Rev. Sci. Instrum. **70**, 4238 (1999).
[16] M. Krems, J. Zirbel, M. Thomason, and R. D. DuBois, Rev. Sci. Intrum. **76**, 093305 (2005).
[17] I. Yu. Tolstikhina, S. S. Churilov, A. N. Ryabtsev, and K. N. Koshelev, *EUV Sources for Lithography*, edited by V. Bakshi (SPIE, Bellingham, 2006), Chap. 4.
[18] D. Ryutov, M. S. Derzon, and M. K. Matzen, Rev. Mod. Phys. **72**, 167 (2000).